Journal of Asian Ceramic Societies 3 (2015) 221–229

HOSTED BY

Contents lists available at ScienceDirect

Journal of Asian Ceramic Societies

journal homepage: www.elsevier.com/locate/jascer

Review Article

Development of high-thermal-conductivity silicon nitride ceramics

You Zhou*, Hideki Hyuga, Dai Kusano[1], Yu-ichi Yoshizawa, Tatsuki Ohji, Kiyoshi Hirao

National Institute of Advanced Industrial Science and Technology (AIST), Nagoya 463-8560, Japan

ARTICLE INFO

Article history:
Received 13 January 2015
Received in revised form 23 March 2015
Accepted 23 March 2015
Available online 7 April 2015

Keywords:
Silicon nitride
Thermal conductivity
Reaction-bonding
Nitridation

ABSTRACT

Silicon nitride (Si_3N_4) with high thermal conductivity has emerged as one of the most promising substrate materials for the next-generation power devices. This paper gives an overview on recent developments in preparing high-thermal-conductivity Si_3N_4 by a sintering of reaction-bonded silicon nitride (SRBSN) method. Due to the reduction of lattice oxygen content, the SRBSN ceramics could attain substantially higher thermal conductivities than the Si_3N_4 ceramics prepared by the conventional gas-pressure sintering of silicon nitride (SSN) method. Thermal conductivity could further be improved through increasing the β/α phase ratio during nitridation and enhancing grain growth during post-sintering. Studies on fracture resistance behaviors of the SRBSN ceramics revealed that they possessed high fracture toughness and exhibited obvious *R*-curve behaviors. Using the SRBSN method, a Si_3N_4 with a record-high thermal conductivity of 177 $Wm^{-1}K^{-1}$ and a fracture toughness of 11.2 MPa $m^{1/2}$ was developed. Studies on the influences of two typical metallic impurity elements, Fe and Al, on thermal conductivities of the SRBSN ceramics revealed that the tolerable content limits for the two impurities were different. While 1 wt% of impurity Fe hardly degraded thermal conductivity, only 0.01 wt% of Al caused large decrease in thermal conductivity.

Contents

1. Introduction 221
2. Thermal conductivity of silicon nitride 222
3. High-thermal-conductivity silicon nitride via the SRBSN route 222
4. Fracture Toughness of High-Thermal-Conductivity Silicon Nitride Ceramics 225
5. Effects of metallic impurity elements on thermal conductivity of SRBSN ceramics 226
   5.1. Effects of impurity iron 226
   5.2. Effects of impurity aluminum 226
6. Summary 227
   Acknowledgements 229
   References 229

1. Introduction

Energy and environment-related problems are serious social issues. In order to save energy as well as to reduce the emission of carbon dioxide, energy sources tend to shift from fossil fuel to electric power, hence highly efficient use of electric power becomes more and more important. Power electronic devices are key technologies for this purpose, and they have been widely used for a variety of applications such as industrial robots, hybrid motor vehicles, and advanced electric trains [1]. Driven by the demand for more efficient control and conversion of electric power, power device technology is advancing toward higher voltage, larger current, greater power density, and this trend is poised to be accelerated with the replacement of Si by the wide-band gap semiconductors (SiC and GaN) in the near future [2,3]. However, the high power will induce large thermal stresses in the devices, which poses great challenges for the assembly of the devices and the

* Corresponding author. Tel.: +81 527367102.
E-mail address: you.zhou@aist.go.jp (Y. Zhou).
[1] Japan Fine Ceramics Co., Ltd., Sendai, 981-3203, Japan.
Peer review under responsibility of The Ceramic Society of Japan and the Korean Ceramic Society.

http://dx.doi.org/10.1016/j.jascer.2015.03.003

packaging materials, especially the brittle ceramic substrates that provide functions of electrical insulation and heat dissipation. Therefore, both good mechanical reliability and high thermal conductivity are required for the ceramic substrates used for the high-power electronic devices.

So far, AlN has been used as a major ceramic substrate material for power devices because it exhibits high thermal conductivity over 200 $Wm^{-1} K^{-1}$. However, mechanical properties of AlN are not sufficient (generally, bending strength of 300–400 MPa, fracture toughness of 3–4 $MPa\,m^{1/2}$), which results in low reliability of the substrates. The electronic industry is eager to seek alternative high-thermal-conductivity substrate materials with good mechanical properties, therefore attention is turned to Si_3N_4 ceramics.

Over the last decades, Si_3N_4 ceramics have been investigated as high temperature structural materials, and now Si_3N_4 with bending strength over 1 GPa can be prepared by choosing appropriate sintering additives and fully developing a bimodal microstructure composed of interlocked rod-like grains [4]. However, thermal conductivity of Si_3N_4 ceramics is usually rather low (<70 $Wm^{-1} K^{-1}$). If thermal conductivity of Si_3N_4 can be improved and at the mean time its good mechanical properties can be maintained, Si_3N_4 would undoubtedly be an attractive substrate material for high-power electronic device applications. Such an expectation has fascinated many researchers to improve thermal conductivities of Si_3N_4 ceramics by a variety of means in recent years. In this paper, previous studies on thermal conductivity property of Si_3N_4 are briefly reviewed. Following that, some recent achievements of our research group on fabricating high-thermal-conductivity Si_3N_4 ceramics via a reaction-bonding and post-sintering method are introduced.

2. Thermal conductivity of silicon nitride

Si_3N_4 mainly exists in two hexagonal polymorphs, namely α- and β-Si_3N_4, which are generally regarded as low and high temperature crystal forms, respectively [5]. Industrial synthesis routes mainly lead to α-Si_3N_4, which converts to the more stable β-Si_3N_4 phase during high temperature sintering. Si_3N_4 is a highly covalent compound, and it transports heat primarily by phonons at room temperature and below. In 1995, Haggerty and Lightfoot [6] predicted that the intrinsic thermal conductivity of Si_3N_4 might be 200–320 $Wm^{-1} K^{-1}$ at room temperature. Later, Watari et al. [7] estimated that the upper limit of the intrinsic thermal conductivity of β-Si_3N_4 could be 400 $Wm^{-1} K^{-1}$. Moreover, Hirosaki et al. [8] estimated the theoretical thermal conductivity of single crystal α- and β-Si_3N_4, using the molecular dynamics method in conjunction with the Green–Kubo formulation, as a function of temperature. In their calculation, the estimated thermal conductivities of α- and β-Si_3N_4, along the *a*-axis and *c*-axis at room temperature were approximately 105 and 225 $Wm^{-1} K^{-1}$, and 170 and 450 $Wm^{-1} K^{-1}$, respectively. However, thermal conductivities of polycrystalline Si_3N_4 ceramics are much lower than the intrinsic values of the single crystal due to the following reasons.

Owing to its strong covalency and low diffusivity, sinterability of Si_3N_4 is poor. Si_3N_4 is generally densified by liquid-phase-sintering mechanisms, where some oxide sintering aids are added and they react with Si_3N_4 as well as the silica phase on the surface of Si_3N_4 particles to form a liquid phase which promotes densification through rearrangement and solution-reprecipitation mechanisms during sintering. After sintering, the liquid phase converts to glassy or partially crystallized phases (oxynitrides) in the sintered material. They may exist as isolated secondary phases at the triple point junctions surrounded by three grains, or as a continuous thin film (around 1 nm thickness) on the boundaries between two adjacent grains. Because thermal conductivities of these oxynitride secondary phases are quite low (less than 5 $Wm^{-1} K^{-1}$), their existence in the microstructure causes reduction of the thermal conductivity of the sintered material. Compared with the triple-junction phases, the detrimental effect of the grain boundary phases is greater due to its continuity. Kitayama et al. [9] assessed the effects of the grain boundary phases on the overall thermal conductivities of Si_3N_4 ceramics by using a modified Wieners' model, and their calculation indicated that the detrimental effect of the grain boundary phases could be alleviated when the grain sizes of the β-Si_3N_4 grains were larger than several micrometers. Thus, promoting grain growth is an effective way of improving thermal conductivity. However, it should be aware that microstructural coarsening often results in lower mechanical strength of the material.

Besides the secondary and grain boundary phases which reside outside Si_3N_4 grains, there exist a variety of imperfections called lattice defects (impurity atoms, vacancies, dislocations, stacking faults, etc.) within the Si_3N_4 grains. Because Si_3N_4 transports heat primarily by phonon (lattice vibration), lattice defects in Si_3N_4 crystals can induce phonon scattering, thereby reducing thermal conductivity. It has been reported that solution of oxygen into Si_3N_4 crystals generates vacancies at the Si sites in Si_3N_4 lattice [10,11]. Si vacancies can scatter phonons and lead to lower thermal conductivity. In order to improve thermal conductivity, it is essential to lower the content of oxygen dissolved in Si_3N_4 lattice (i.e., lattice oxygen content).

Therefore, choosing a Si_3N_4 powder with low impurity oxygen content as a starting material is decisively important for preparing Si_3N_4 ceramics with high thermal conductivity. Sintering additives, which are indispensible for achieving densification of Si_3N_4, also play an important role in reducing lattice oxygen content of the sintered Si_3N_4. Using sintering additives with high oxygen affinity (e.g., rare earth oxides) [7,12], or choosing sintering additive compositions which lead to high nitrogen/oxygen ratios of the liquid phase during sintering were effective ways of reducing lattice oxygen content of the sintered Si_3N_4. For example, Hayashi et al. [13] reported that while a Si_3N_4 ceramic with a thermal conductivity of 120 $Wm^{-1} K^{-1}$ was prepared by using a Yb_2O_3-MgO sintering additive, the thermal conductivity could be increased to 140 $Wm^{-1} K^{-1}$ by replacing MgO with $MgSiN_2$ in the sintering additive so that nitrogen/oxygen ratio of the liquid phase was increased.

However, for Si_3N_4 starting powders, even the top grade high-purity commercial powder contains more than 1 wt% of oxygen residing both on the surface and within the lattice, which imposes an upper limit on the attainable thermal conductivity of Si_3N_4 ceramics. In order to raise the upper limit to a higher level, a starting powder containing less oxygen should be used. Motivated by such an idea, our research group proposed a strategy of preparing high thermal conductivity Si_3N_4 via a route of sintering of reaction-bonded silicon nitride (SRBSN), which is a well-known process of fabricating Si_3N_4 ceramics from an Si starting powder instead of a Si_3N_4 powder [14–17], in consideration of the fact that Si powders containing much less oxygen and metallic impurities than Si_3N_4 powders are commercially available thanks to the advancement of modern semiconductor industry. Our experimental results have verified the effectiveness of the SRBSN strategy, by which both higher thermal conductivity and higher mechanical strength were achieved, compared to the conventional sintering of silicon nitride powder (SSN) route [18–28].

3. High-thermal-conductivity silicon nitride via the SRBSN route

The sintering of reaction-bonded silicon nitride (SRBSN) method consists of two processing steps. Firstly, an Si compact composed of Si powder and sintering additives is heated to a temperature

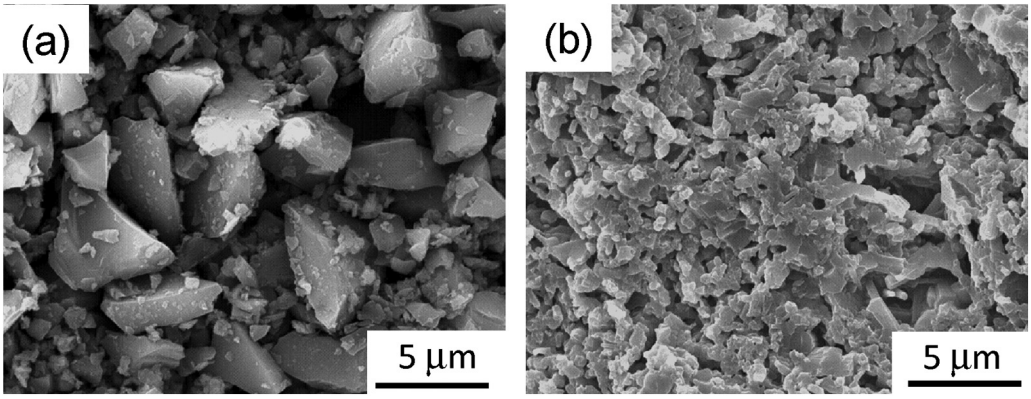

Fig. 1. SEM images of (a) Si raw powder and (b) nitrided compact at 1400 °C [27].

near the melting point of Si (1414 °C) in a nitrogen atmosphere so that the Si compact is nitrided and transforms to a porous Si_3N_4 compact. Then the nitrided compact is further heated to a higher temperature (but below the decomposition temperature of Si_3N_4) so that the porous Si_3N_4 is sintered and turns to a dense Si_3N_4 ceramic. Because Si raw powders are usually cheaper than Si_3N_4 raw powders, compared to the SSN method, the SRBSN method has long been known as a low-cost processing technique of fabricating Si_3N_4 ceramics [14–17]. However, the motivation of using the SRBSN method to prepare Si_3N_4 ceramics with high thermal conductivity was that by this method Si powders containing lower oxygen content than even the high-grade Si_3N_4 powders could be used as the starting materials. Moreover, the whole process from nitridation to post-sintering can be continuously carried out without exposing the compacts to the air, therefore it is favorable for controlling the oxygen content of the post-sintered Si_3N_4.

The attainment of a complete nitridation of Si is the first step and the key to success of a SRBSN process. However, nitridation of Si is actually difficult to control due to the exothermic reaction between Si and N_2 gas. Therefore, we first systematically studied the influences of various parameters such as particle size and purity of Si powders, types and amount of sintering additives and parameters such as heating rate, nitriding temperature and holding time used in the nitridation process [20,29]. The studies showed that full nitridation could be realized through judiciously choosing and controlling various processing parameters.

Based on the aforementioned studies, for the purpose of preparing Si_3N_4 ceramics with high thermal conductivity by the SRBSN method, a high purity Si powder containing less than 0.01 wt% of total metallic impurities and 0.28 wt% of oxygen was chosen as a starting powder. A mixture of Y_2O_3 and MgO was added into the Si powder as sintering additives. The amount of sintering additives was determined so as to give the fully nitrided body a nominal composition of Si_3N_4:Y_2O_3:MgO = 93:2:5 in molar ratio. Si powder and sintering additives were mixed in methanol using a planetary mill in a Si_3N_4 jar with Si_3N_4 balls. After drying and sieving, the mixed powder was uniaxially pressed in a 45 mm × 45 mm stainless-steel die and cold-isostatically pressed at a pressure of 300 MPa. The formed Si compact was placed in a graphite resistance furnace and nitrided at 1400 °C for 4 h under a nitrogen pressure of 0.1 MPa. X-ray diffraction analysis (XRD) on the nitrided compact revealed that there was no diffraction peaks of Si, indicating that the Si compact was completely nitrided. The main crystalline phases were β- and α-Si_3N_4 and the minor phases were $Y_2Si_3O_3N_4$ and $YSiO_2N$. Quantitative XRD analysis further revealed that the content ratio of β-Si_3N_4 to α-Si_3N_4 was 59.8 to 40.2. Scanning electron microscopic (SEM) observation showed that the Si_3N_4 grains in the nitrided compact became much finer than the starting Si powder particles (Fig. 1). The nitrided compact had a relative density near 75%. In contrast, when starting from fine Si_3N_4 powders, it is difficult to attain a green density over 60% even if using a CIPping pressure as high as 400 MPa. The high density of the nitrided body is beneficial for promoting densification and shortening sintering time in the next step of post-sintering.

Post-sintering of the nitrided compact was done at 1900 °C for various times ranging from 3 to 48 h under 1 MPa nitrogen pressure. SEM images (Fig. 2) of the fracture surfaces of the sintered materials showed some common features: fibrous and faceted grain shapes and a bimodal microstructure where a small fraction of large grains were embedded in a majority of small grains. With increasing sintering time, the microstructures became coarser. For the materials sintered for 3 or 6 h, the microstructures were generally fine, though a few large fibrous grains had lengths of around 10 μm. After being sintered for 12 or 24 h, many grains grew to lengths of over 10 μm.

The SRBSN materials sintered for 3, 6, 12, 24, and 48 h had thermal conductivities of 100, 105, 117, 133, and 142 $Wm^{-1}\,K^{-1}$, respectively. For the sake of comparison, Si_3N_4 ceramics were also prepared by the conventional SSN method using the same sintering additives and same sintering parameters as those used for post-sintering of the SRBSN materials. In this case, the starting powder was a fine α-Si_3N_4 powder containing 1.2 wt% of oxygen, and these Si_3N_4 ceramics were termed as SSN materials. The SSN materials sintered for 3, 6, 12, 24, and 48 h had thermal conductivities of 87, 91, 96, 103, and 111 $Wm^{-1}\,K^{-1}$, respectively. The thermal conductivities of both the SRBSN and the SSN materials were plotted against the sintering times in Fig. 3, which clearly showed that when sintered for the same length of time, the SRBSN materials always had higher thermal conductivities than the SSN counterpart materials; when sintering time was longer, the differences in thermal conductivity between the SRBSN and SSN materials became larger.

Flexural strength was measured using test beams with dimensions of 4 mm × 3 mm × 36 mm, which were machined from the sintered materials and tested in a four-point bending jig with an outer span of 30 mm and an inner span of 10 mm. The measured strength values of the SRBSN and the SSN materials sintered for various lengths of time, together with their thermal conductivities, were plotted in Fig. 4. For comparison, data of thermal conductivity and bending strength of some other high-thermal-conductivity SSN materials reported in literature were also included in the graph [30,31]. It can be seen that the SRBSN materials had a better balance between thermal conductivity and bending strength compared to the SSN materials. That could be due to the lower oxygen content of the Si starting powder used for the SRBSN method than that of the Si_3N_4 starting powder used for the SSN method. The lower

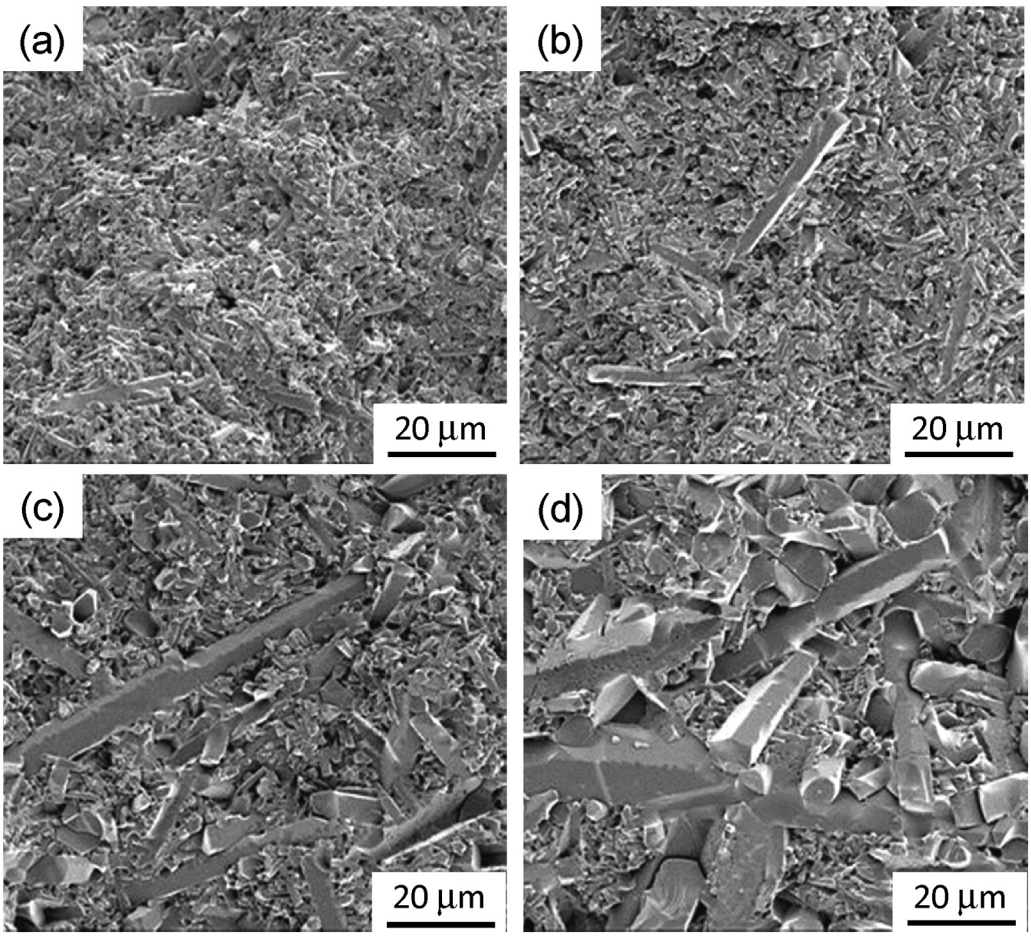

Fig. 2. SEM images of fracture surfaces of SRBSN sintered for various times: (a) 3 h, (b) 6 h, (c) 12 h and (d) 24 h [27].

oxygen content of the starting material led to lower lattice oxygen content of the SRBSN materials, which could attain a higher thermal conductivity when sintered for shorter times compared to the SSN materials. And, a shorter-time sintering would result in a finer microstructure and a higher flexural strength. Therefore, Si_3N_4 ceramics with both high thermal conductivity and high mechanical strength could be fabricated by the SRBSN method.

As mentioned above, compared to the SSN materials, the higher thermal conductivities of the SRBSN materials were attributed to the lower oxygen content of the starting material (Si powder vs Si_3N_4 powder), which resulted in lower lattice oxygen content

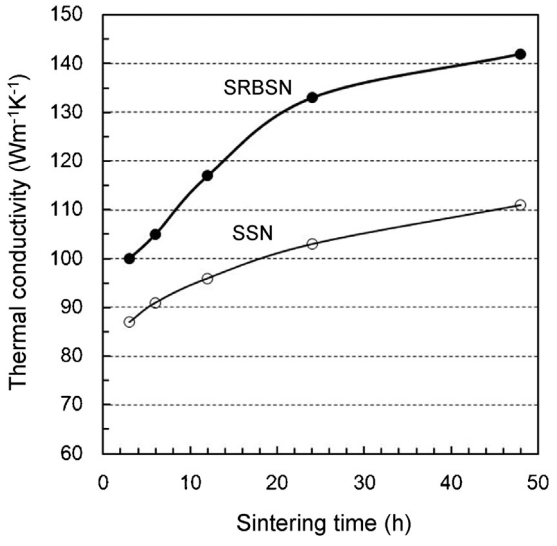

Fig. 3. Thermal conductivities of the sintered reaction-bonded Si_3N_4 (SRBSN) and the gas-pressure sintered Si_3N_4 (SSN) sintered at 1900 °C for various lengths of time.

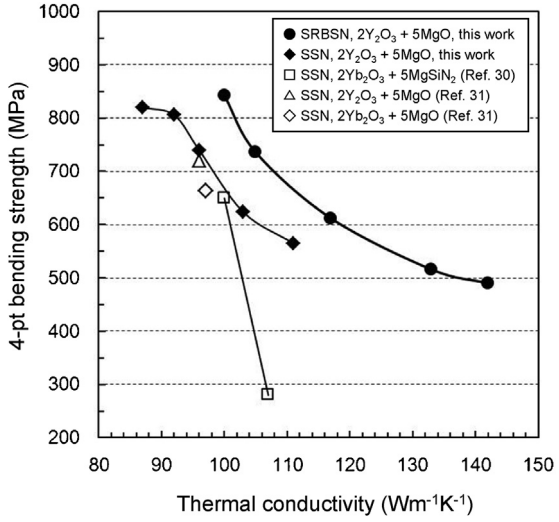

Fig. 4. Relation between thermal conductivity and bending strength for the sintered reaction-bonded Si_3N_4 (SRBSN) and the gas-pressure sintered Si_3N_4 (SSN) prepared in this work and some gas-pressure sintered Si_3N_4 reported in literature.

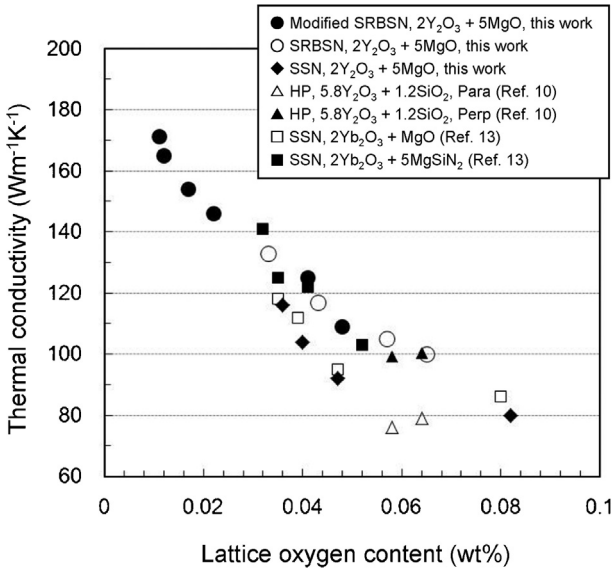

Fig. 5. Relation between thermal conductivity and lattice oxygen content for the sintered reaction-bonded Si_3N_4 (SRBSN) and the gas-pressure sintered Si_3N_4 (SSN) prepared in this work and some Si_3N_4 densified by hot-pressing (HP) or gas-pressure sintering reported in literature.

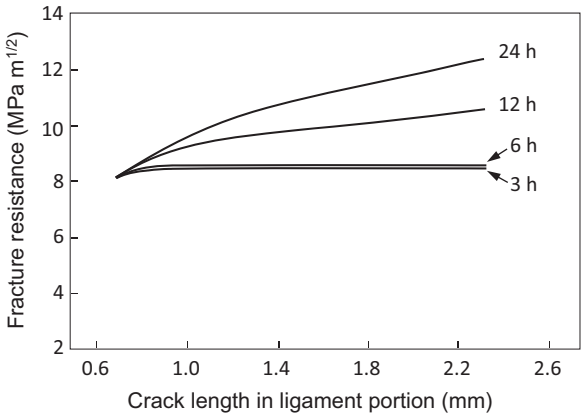

Fig. 6. Fracture resistance as a function of crack extension obtained in chevron-notched-beam tests for the SRBSN materials sintered for 3, 6, 12, and 24 h [28].

of the Si_3N_4 grains after nitridation and post-sintering. Later, we found that the lattice oxygen content of the Si_3N_4 grains could be further reduced to a lower level through modifying the nitridation process [23]. The nitridation condition was modified by creating a more reducing atmosphere in the reaction zone so as to obtain a higher β:α Si_3N_4 ratio. For example, the modified nitridation could result in a Si_3N_4 compact with a β:α ratio of 82.5:17.5. The measured lattice oxygen content of the Si_3N_4 grains in this nitrided compact was 0.115 wt%. In contrast, the lattice oxygen content of the aforementioned nitrided compact which had a β:α Si_3N_4 ratio of 59.8:40.2 was 0.142 wt%. This result proved our assumption that lattice oxygen content of the resultant Si_3N_4 could be reduced by promoting formation of β phase during nitridation of Si.

The nitrided compacts prepared by the modified nitridation process were post-sintered at 1900 °C for various lengths of time. The Si_3N_4 ceramics sintered for 3, 6, 12, and 24 h had thermal conductivities of 109, 125, 146, and 154 $Wm^{-1}K^{-1}$, respectively. In contrast, as mentioned above, the Si_3N_4 ceramics sintered from the nitrided compact with a β:α ratio of 59.8:40.2 for 3, 6, 12, and 24 h had thermal conductivities of 100, 105, 117, and 133 $Wm^{-1}K^{-1}$, respectively. The improvement in thermal conductivity of the Si_3N_4 sintered from the nitrided compacts with a higher β:α ratio was remarkable. Lattice oxygen measurement revealed that the Si_3N_4 ceramics sintered from the high β nitrided compact for 3, 6, 12, and 24 h had lattice oxygen contents of 0.048, 0.041, 0.022, and 0.017 wt%, respectively. In contrast, the Si_3N_4 ceramics sintered from the low β nitrided compact had lattice oxygen contents of 0.065, 0.057, 0.043, and 0.033 wt%, respectively. Microstructural observations showed that these two types of Si_3N_4 (i.e., sintered from high β and low β RBSN compacts) had similar microstructures when they were sintered for the same length of time. Therefore, the higher thermal conductivities of the Si_3N_4 ceramics sintered from the higher β RBSN compact could be attributed to their lower lattice oxygen contents. It was found that even higher thermal conductivity could be attained through further reducing lattice oxygen content by prolonging sintering time. For example, a Si_3N_4 prepared by sintering a high β RBSN compact at 1900 °C for 60 h and then cooling at a rate of 0.2 °C min^{-1} attained a record-high thermal conductivity of 177 $Wm^{-1}K^{-1}$.

Fig. 5 shows relationship between thermal conductivities and lattice oxygen contents for the Si_3N_4 ceramics prepared by the SSN, SRBSN and modified SRBSN methods. For comparison, data of thermal conductivity and lattice oxygen content of some Si_3N_4 ceramics which were added with various kinds of sintering additives and densified by hot-pressing or gas-pressure sintering reported in literature were also included in the graph [10,13]. Despite of the various sintering additives and sintering methods, the data showed a clear tendency that thermal conductivity increased with decreasing lattice oxygen content. For different sintering additives and sintering methods, the prepared Si_3N_4 might have different thermal conductivities even if their lattice oxygen contents were similar. That was due to the influences of some microstructural factors (grain size, grain boundary phase, grain orientation, etc.) [10,13]. However, as shown in Fig. 5, those influences were secondary to the effect of lattice oxygen content on thermal conductivity. The clear tendency shown in Fig. 5 indicated that lattice oxygen was the crucial factor governing thermal conductivity of Si_3N_4 ceramics.

4. Fracture Toughness of High-Thermal-Conductivity Silicon Nitride Ceramics

For the application as substrates for the next-generation power devices, not only high thermal conductivity and high strength of the substrate materials are required, but also high fracture toughness is demanded. We studied the fracture toughness property of the aforementioned high thermal conductivity SRBSN materials, which were sintered at 1900 °C for various lengths of time ranging from 3 to 24 h. Fracture resistance behavior (*R*-curve) was evaluated by the chevron-notched-beam (CNB) test method [32], and fracture toughness was measured by both the CNB method and the single-edge-precrackedbeam (SEPB) method [33]. As shown in Table 1, for all the materials, their fracture toughness values measured by the CNB and the SEPB methods were nearly the same. It is worth noting that the material sintered for 3 h already attained a fracture toughness as high as 8.4 MPa $m^{1/2}$. The fracture toughness values became higher for the materials sintered for longer times, especially when the sintering times were longer than 12 h. The material sintered for 24 h possessed a fracture toughness of 10.7 MPa $m^{1/2}$ [28].

Fig. 6 shows the *R*-curves of the SRBSN materials sintered for 3, 6, 12, and 24 h, which were measured and recorded after cracks extended for about 0.65 mm in the ligament portions of the CNB test specimens. On the *R*-curves of the materials sintered for 3 and 6 h, small increments were observed during cracks growing from 0.65 mm to about 1.0 mm. After that the *R*-curves became almost flat and the fracture resistance values were nearly constant, which

Table 1
Properties of the SRBSN ceramics sintered at 1900 °C for various lengths of time.

Sintering time (h)	Relative density (%)	Thermal conductivity ($W m^{-1} K^{-1}$)	Bending strength (MPa)	Fracture toughness (by CNB) ($MPa m^{1/2}$)	Fracture toughness (by SEPB) ($MPa m^{1/2}$)
3	99.3	109	786 ± 17	8.42 ± 0.23	8.44 ± 0.03
6	99.4	125	676 ± 21	8.47 ± 0.02	8.57 ± 0.16
12	99.1	146	608 ± 12	9.99 ± 0.10	9.66 ± 0.10
24	98.5	154	505 ± 9	10.63 ± 0.37	10.73 ± 0.18

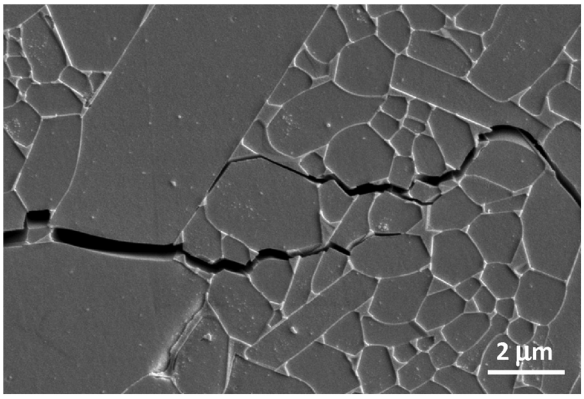

Fig. 7. A scanning electron microscopic view of a crack path (propagating from left to right) in an SRBSN material sintered at 1900 °C for 24 h [28].

were 8.4 and 8.6 $MPa m^{1/2}$ for the materials sintered for 3 and 6 h, respectively. On the other hand, the materials sintered for 12 and 24 h showed rising *R*-curve behaviors. The fracture resistance values exceeded 10 and 12 $MPa m^{1/2}$ for the materials sintered for 12 and 24 h, respectively, at the point close to the complete separation of the test beams.

These results revealed that the SRBSN materials sintered with Y_2O_3 and MgO additives could not only attain high thermal conductivity but also possess exceptionally high fracture toughness, in comparison with most Si_3N_4 ceramics reported in literature which were usually sintered by using a combination of Al_2O_3 and other oxides as sintering additives. The high fracture toughness was thought to be attributed to an appropriately weak grain boundary which would favor interfacial debonding and facilitate toughening effects such as crack-bridging and crack-deflection. Fig. 7 shows a scanning electron microscopic view of a crack path in an SRBSN material sintered for 24 h. Interfacial debonding extensively occurred, causing a crack to propagate tortuously and leading to crack-bridging and crack-deflection toughening effects.

5. Effects of metallic impurity elements on thermal conductivity of SRBSN ceramics

Although choosing a high-purity Si powder as the starting material is essential for preparing high-thermal-conductivity Si_3N_4 ceramics by the SRBSN method, a reagent-grade Si starting powder is often too expensive for industrial production. From the standpoint of practical application, it is necessary to study the thermal conductivity of SRBSN ceramics prepared from industrial grade Si powders, which usually contain some metallic impurity elements. Fe and Al are the two most popular metallic impurity elements in Si powders, due to contamination in the milling process by which coarse Si grits are pulverized to fine Si powders. Kusano et al. [34,35] studied the influences of Fe and Al impurity elements of Si starting powders on the thermal conductivity of the prepared SRBSN ceramics.

5.1. Effects of impurity iron

A high-purity Si powder (purity > 99.99%, major metallic impurities: 49 ppm of Fe and 37 ppm of Al) was chosen as the starting material, and 2 mol% of Y_2O_3 and 5 mol% of $MgSiN_2$ were used as sintering additives. Various amount of Fe powder were added into the Si powder in order to investigate the effects of impurity Fe on the properties of SRBSN ceramics. The specimens added with 0, 0.1, 1.0, and 5.0 wt% of Fe were designated as F0, F0.1, F1, and F5, respectively [34]. Nitridation was carried out at 1400 °C for 8 h under a nitrogen pressure of 0.1 MPa, and post-sintering of the nitrided samples was done at 1900 °C for 6 h under a nitrogen pressure of 0.9 MPa. The relative densities of the sintered specimens F0, F0.1, F1, and F5 were 99.8%, 99.8, 99.5%, and 98.4%, respectively. SEM observation (Fig. 8) on the polished and plasma-etched surfaces revealed that all the SRBSN ceramics were basically made up of rod-like β-Si_3N_4 grains, while some equiaxed $SiFe_x$ particles (as confirmed by XRD analysis) were dispersed in specimens F1 and F5, and they obviously had suppressed the grain growth of β-Si_3N_4 grains.

Specimens F0, F0.1, F1, and F5 had 4-point bending strength values of 770, 756, 758, and 733 MPa, and fracture toughness values of 7.1, 7.5, 6.6, and 6.5 $MPa m^{1/2}$, respectively. The lower fracture toughness of specimens F1 and F5 might be attributed to their finer microstructures. The thermal conductivities of specimens F0, F0.1, F1, and F5 were 82, 81, 80, and 53 $Wm^{-1} K^{-1}$, respectively. It implied that impurity Fe might not have obvious detrimental effect on the thermal conductivity of the SRBSN ceramics when their content was less than 1 wt%, but thermal conductivity could be significantly decreased when the amount of Fe was higher than 1 wt%.

5.2. Effects of impurity aluminum

In order to investigate the effect of impurity Al on the properties of SRBSN ceramics, Kusano et al. [35] added various amount of AlN into a mixture of a high-purity Si starting powder (purity > 99.99%, major metallic impurities: 49 ppm of Fe and 37 ppm of Al) and sintering additives of 2 mol% of Y_2O_3 and 5 mol% of $MgSiN_2$. The contents of AlN additive were adjusted to be 0.01, 0.1, 0.2, and 0.4 wt% of Al relative to Si, and the corresponding specimens were denoted as Al-1, Al-2, Al-3, and Al-4, respectively. The specimen without Al addition was denoted as Al-0.

For all the compositions, full nitridation were achieved when nitriding was done at 1400 °C for 8 h under a nitrogen pressure of 0.1 MPa. And all specimens were almost fully densified when post-sintering was done at 1900 °C for 6 h under a nitrogen pressure of 0.9 MPa. The relative densities of the sintered specimens Al-0, Al-1, Al-2, Al-3, and Al-4 were 99.8%, 99.1%, 99.1%, 99.1%, and 98.5%, respectively. SEM images (Fig. 9) showed that the microstructures of the specimens were composed of coarse prismatic grains and fine grains, and the number of coarse grains became smaller when more Al was added. An image analysis revealed that the average aspect ratios of the β-Si_3N_4 grains were 2.55, 2.21, 1.93, 1.81, and 1.75 in the sintered specimens Al-0, Al-1, Al-2, Al-3, and Al-4, respectively,

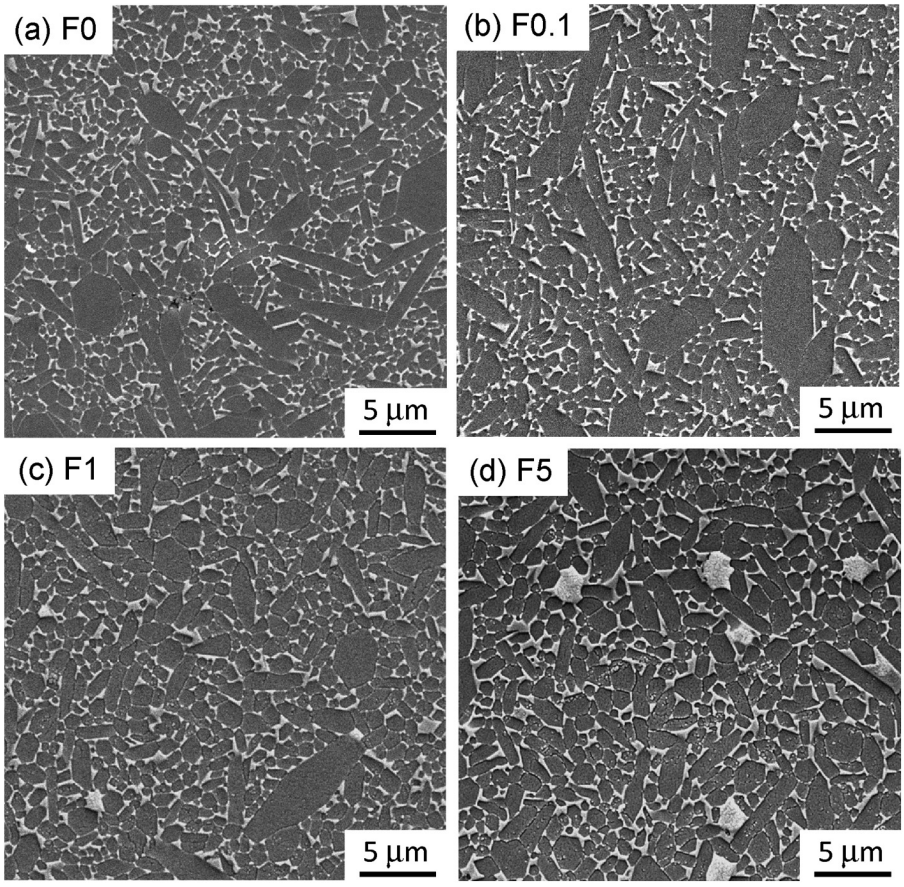

Fig. 8. SEM images of polished and plasma-etched surfaces of the SRBSN materials added with various amount of Fe: (a) F0, (b) F0.1, (c) F1, and (d) F5 [34].

revealing that the aspect ratios deceased with increasing Al additive contents.

As shown in Table 2, all specimens exhibited similar four-point bending strength values of 800–850 MPa, but there were obvious differences in their fracture toughness values. The fracture toughness values of specimens Al-0, Al-1, Al-2, Al-3, and Al-4 were 7.3, 7.1, 6.7, 6.1, 6.0 MPa $m^{1/2}$, respectively, indicating a tendency of decreasing fracture toughness with increasing Al dopant, which was regarded to be due to the existence of fewer coarse elongated β-Si_3N_4 grains in the microstructures of the specimens doped with more Al element.

The thermal conductivities of specimens Al-0, Al-1, Al-2, Al-3, and Al-4 were 91.9, 83.7, 74.1, 66.2, and 58.0 $Wm^{-1}K^{-1}$, respectively. It showed that thermal conductivity drastically decreased with increasing amount of Al additive, and even adding 0.01 wt% of Al could result in considerable decrease of thermal conductivity. This is in contrast with the aforementioned influence of impurity Fe on thermal conductivity of SRBSN ceramics, where 1 wt% of Fe additive did not cause obvious decrease of thermal conductivity.

Kusano et al. [35] claimed that the added Al, together with impurity oxygen, dissolved in the lattice of β-Si_3N_4 and formed β-SiAlON solid solution, i.e., $Si_{6-z}Al_zO_zN_{8-z}$. They measured the contents of Al and O in the lattice of β-Si_3N_4 grains, and then calculated the *Z* values for all the SRBSN specimens. Fig. 10 shows the relationship between thermal conductivities and the corresponding *Z* values. Thermal conductivities decreased with increasing *Z* values. It is worth to note that the thermal conductivities significantly decreased in the region with *Z* values even smaller than 0.03. The fact that trace Al addition resulted in large reduction in thermal conductivity implied that the detrimental influence of impurity Al element on thermal conductivity of SRBSN ceramics could be huge. In other words, for the purpose of preparing high thermal conductivity SRBSN ceramics the tolerable limit of the content of impurity Al in Si starting powder is very low.

6. Summary

Previous studies have indicated that lattice oxygen was the dominant factor lowering the thermal conductivity of Si_3N_4 ceramics. In order to improve thermal conductivity through reducing lattice oxygen content, we used the sintering of reaction-bonded silicon nitride (SRBSN) method to prepare Si_3N_4 ceramics employing high purity silicon as the starting material. Compared to the conventional sintering of silicon nitride (SSN) method,

Table 2
Properties of the SRBSN ceramics added with various amount of Al.

Specimen	Relative density (%)	Thermal conductivity ($Wm^{-1}K^{-1}$)	Bending strength (MPa)	Fracture toughness (MPa $m^{1/2}$)
Al-0	99.8	91.9	801 ± 72	7.3 ± 0.3
Al-1	99.1	83.7	829 ± 23	7.1 ± 0.2
Al-2	99.1	74.1	841 ± 43	6.7 ± 0.5
Al-3	99.1	66.2	841 ± 95	6.1 ± 0.2
Al-4	98.5	58.0	853 ± 90	6.0 ± 0.1

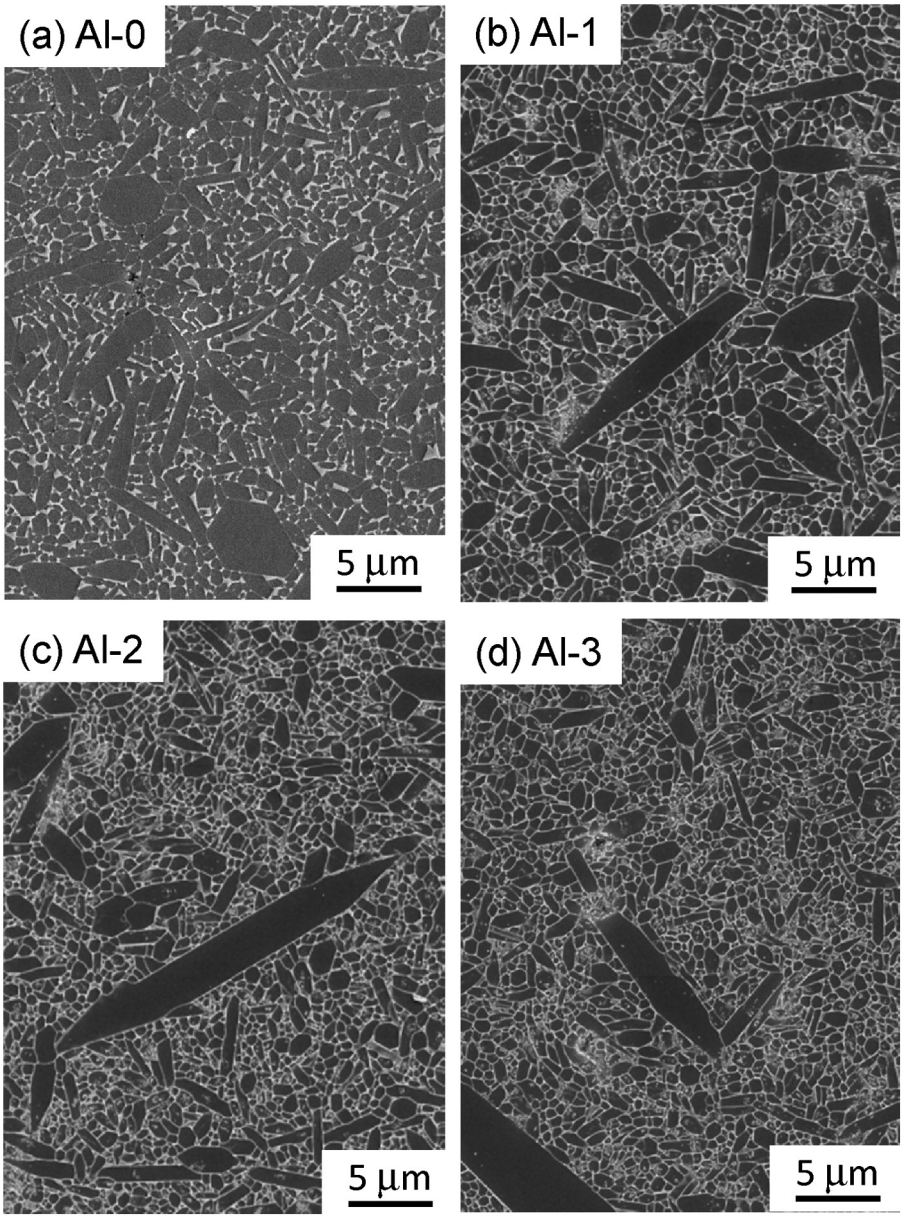

Fig. 9. SEM images of polished and plasma-etched surfaces of the SRBSN materials added with various amount of Al: (a) Al-0, (b) Al-1, (c) Al-2, and (d) Al-3 [35].

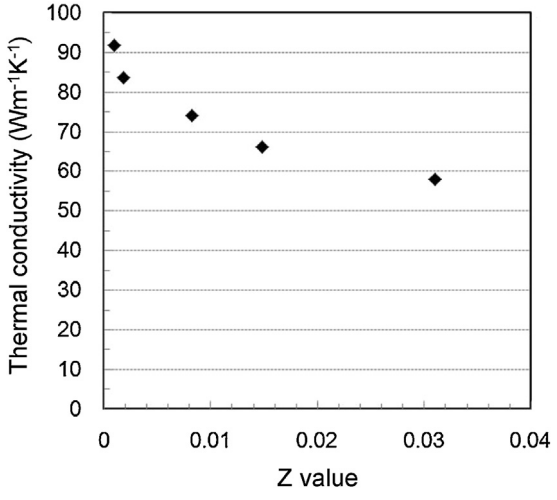

Fig. 10. Relationship between thermal conductivity and *Z* value.

content of impurity oxygen dissolved in Si_3N_4 lattice became lower and the SRBSN ceramics could attain substantially higher thermal conductivities and higher mechanical strength. Furthermore, thermal conductivity could be improved through increasing the β/α phase ratio during nitridation and enhancing grain growth during post-sintering. Studies on fracture resistance behaviors of the high-thermal-conductivity SRBSN ceramics revealed that they possessed high fracture toughness and exhibited *R*-curve behaviors. Using the SRBSN method, a silicon nitride with a record-high thermal conductivity of 177 $Wm^{-1} K^{-1}$ and a fracture toughness of 11.2 MPa $m^{1/2}$ was developed. The influences of impurity Fe and Al elements on thermal conductivities of SRBSN ceramics were studied, and the results revealed that the tolerable content limits for Fe and Al impurities were 1 wt% and 0.01 wt%, respectively. The concurrent attainment of high thermal conductivity and good mechanical properties of the SRBSN ceramics will make them promising candidates for the application as insulating substrates for the next-generation power devices.

Acknowledgements

Part of this research work was carried out under the Novel Semiconductor Power Electronics Projects Realizing Low Carbon-Emission Society (Development of High-Temperature Components and Packaging Technology for SiC Power Modules) promoted by New Energy and Industrial Technology Development Organization (NEDO), Japan.

References

[1] The Institute of Electrical Engineers of Japan, Power Semiconductor That Runs the World (in Japanese), Ohmsha, Ltd., Tokyo (2009).
[2] H. Okumura, Jpn. J. Appl. Phys., 45, 7565–7568 (2005).
[3] C.R. Eddy Jr. and D.K. Gaskill, Science, 324, 1398–1400 (2009).
[4] P.F. Becher, E.Y. Sun, K.P. Plucknett, K.B. Alexander, C.H. Hsueh, H.T. Lin, S.B. Waters, C.G. Westmoreland, E.S. Kang, K. Hirao and M.E. Brito, J. Am. Ceram. Soc., 81, 2821–2830 (1998).
[5] S. Hampshire, H.K. Park, D.P. Thompson and K.H. Jack, Nature, 274, 880–882 (1978).
[6] J.S. Haggerty and A. Lightfoot, Ceram. Eng. Sci. Proc., 16, 475–487 (1995).
[7] K. Watari, J. Ceram. Soc. Jpn., 109, S7–S16 (2001).
[8] N. Hirosaki, S. Ogata, C. Kocer, H. Kitagawa and Y. Nakamura, Phys. Rev. B, (2002), Article No. 134110.
[9] M. Kitayama, K. Hirao, M. Toriyama and S. Kanzaki, J. Am. Ceram. Soc., 82, 3105–3112 (1999).
[10] M. Kitayama, K. Hirao, A. Tsuge, K. Watari, M. Toriyama and S. Kanzaki, J. Am. Ceram. Soc., 83, 1985–1992 (2000).
[11] K. Hirao, K. Watari, H. Hayashi and M. Kitayama, MRS Bull., 26, 451–455 (2001).
[12] M. Kitayama, K. Hirao, K. Watari, M. Toriyama and S. Kanzaki, J. Am. Ceram. Soc., 84, 353–358 (2001).
[13] H. Hayashi, K. Hirao, M. Toriyama, S. Kanzaki and K. Itatani, J. Am. Ceram. Soc., 84, 3060–3062 (2001).
[14] A.J. Moulson, J. Mater. Sci., 14, 1017–1051 (1979).
[15] G. Ziegler, J. Heinrich and G. Wotting, J. Mater. Sci., 22, 3041–3086 (1987).
[16] F.L. Riley, J. Am. Ceram. Soc., 83, 245–265 (2000).
[17] B.T. Lee, J.H. Yoo and H.D. Kim, Mater. Sci. Eng. A, 333, 306–313 (2002).
[18] X.W. Zhu, Y. Zhou, K. Hirao and Z. Lences, J. Am. Ceram. Soc., 89, 3331–3339 (2006).
[19] X.W. Zhu, Y. Zhou, K. Hirao and Z. Lences, J. Am. Ceram. Soc., 90, 1684–1692 (2007).
[20] Y. Zhou, X.W. Zhu, K. Hirao and Z. Lences, Int. J. Appl. Ceram. Technol., 5, 119–126 (2008).
[21] K. Hirao and Y. Zhou, R. Riedel and I.W. Chen, Ceramics Science and Technology, vol. 2, Wiley-VCH, Weinheim, (2010) pp. 667–696.
[22] K. Hirao, Bull. Ceram. Soc. Jpn., 45, 444–447 (2010).
[23] Y. Zhou, H. Hyuga, D. Kusano, Y. Yoshizawa and K. Hirao, Adv. Mater., 23, 4563–4567 (2011).
[24] Y. Zhou, K. Hirao, H. Hyuga and D. Kusano, Ceram. Eng. Sci. Proc., 32, 27–33 (2011).
[25] K. Hirao, Y. Zhou, H. Hyuga, T. Ohji and D. Kusano, J. Korean Ceram. Soc., 49, 380–384 (2012).
[26] Y. Zhou and H. Hyuga, Bull. Ceram. Soc. Jpn., 47, 12–17 (2012).
[27] Y. Zhou, H. Hyuga, T. Ohji and K. Hirao, Ceram. Eng. Sci. Proc., 34, 79–88 (2013).
[28] Y. Zhou, T. Ohji, H. Hyuga, Y. Yoshizawa, N. Murayama and K. Hirao, Int. J. Appl. Ceram. Technol., 11, 872–882 (2014).
[29] X.W. Zhu, Y. Zhou and K. Hirao, J. Mater. Sci., 39, 5785–5797 (2004).
[30] H. Hayashi, K. Hirao, Y. Yamauchi and S. Kanzaki, Proc. Annu. Meeting Ceram. Soc. Jpn., (2003), pp. 248.
[31] X.W. Zhu, H. Hayashi, Y. Zhou and K. Hirao, J. Mater. Res., 19, 3270–3278 (2004).
[32] T. Ohji, Y. Goto and A. Tsuge, J. Am. Ceram. Soc., 74, 739–745 (1991).
[33] T. Nose and T. Fujii, J. Am. Ceram. Soc., 71, 328–333 (1988).
[34] D. Kusano, Y. Noda, H. Shibasaki, H. Hyuga, Y. Zhou and K. Hirao, Int. J. Appl. Ceram. Technol., 10, 690–700 (2013).
[35] D. Kusano, H. Hyuga, Y. Zhou and K. Hirao, Int. J. Appl. Ceram. Technol., 11, 534–542 (2014).